Supplemental Material for "Fluid viscoelasticity affects ultrasound force field induced particle transport"

T. Sujith, L. Malik and A. K. Sen†

Micro Nano Bio Fluidics Unit, Department of Mechanical Engineering, Indian Institute of Technology Madras, Chennai-600036, India

1. Theoretical modelling

1.1. *Acoustic boundary layer thickness and viscous wavelength formulation*

The continuity and momentum equations are

$$\frac{\partial \rho_1}{\partial t} + \rho_0 \boldsymbol{\nabla} \cdot \boldsymbol{v}_1 = 0, \tag{1.1}$$

$$\rho_0 \frac{\partial \boldsymbol{v}_1}{\partial t} = -\boldsymbol{\nabla} p_1 + \boldsymbol{\nabla} \cdot \mu_c \left[\boldsymbol{\nabla} \boldsymbol{v}_1 + (\boldsymbol{\nabla} \boldsymbol{v}_1)^T - \frac{2}{3} (\boldsymbol{\nabla} \cdot \boldsymbol{v}_1) \boldsymbol{I} \right], \tag{1.2}$$

where

$$\mu_c = \mu_s + \frac{\mu_p}{1 + i\tau\omega}. \tag{1.3}$$

The equation of state can be expressed as

$$p_1 - p_0 = (\rho_1 - \rho_0) c_0^2, \tag{1.4}$$

The first order velocity can be represented in terms of potential (φ_p) and stream function ($\boldsymbol{\Psi}$) as (Doinikov *et al.* 2021*a*):

$$\boldsymbol{v}_1 = \boldsymbol{\nabla}\varphi_{p1} + \boldsymbol{\nabla} \times \boldsymbol{\Psi}_1 \tag{1.5}$$

Substituting equation (1.5) in equations (1.1), (1.2), and (1.4), further simplification gives,

$$\nabla^2 \varphi_{p1} + k_f^2 \varphi_{p1} = 0 \tag{1.6}$$

and

$$\nabla^2 \boldsymbol{\Psi}_1 + k_{ve}^2 \boldsymbol{\Psi}_1 = 0. \tag{1.7}$$

Where k_f and k_{ve} are wave numbers, given by

$$k_{ve} = (1-i)\sqrt{\frac{\rho_0\omega}{2\mu_c}} \quad \text{and} \quad k_f = \frac{\omega}{c}\left[1 + \frac{i\omega}{\rho_0 c^2}\frac{4\mu_c}{3}\right]^{-\frac{1}{2}}. \tag{1.8}$$

By following the similar analogy of viscous fluid, magnitude of boundary layer thickness and viscous wavelength for viscoelastic fluid can be expressed as (Doinikov *et al.* 2021*a*),

$$\delta_{ve} = -\frac{1}{\text{Im}\{k_{ve}\}} \quad \text{and} \quad \lambda_{ve} = \frac{2\pi}{\text{Re}\{k_{ve}\}}. \tag{1.9}$$

† Email address for correspondence: ashis@iitm.ac.in

1.2. *Acoustic radiation force derivation in the far field*

We begin the derivation of the acoustic radiation force expression by considering the time-averaged second-order field equations,

$$\rho_0 \boldsymbol{\nabla} \cdot \langle \boldsymbol{v}_2 \rangle = -\boldsymbol{\nabla} \cdot \langle \rho_1 \boldsymbol{v}_1 \rangle \tag{1.10}$$

and

$$\langle \rho_1 \partial_t \boldsymbol{v}_1 \rangle + \rho_0 \langle \boldsymbol{v}_1 \cdot \boldsymbol{\nabla} \boldsymbol{v}_1 \rangle = -\boldsymbol{\nabla} \langle p_2 \rangle + \mu \boldsymbol{\nabla}^2 \langle \boldsymbol{v}_2 \rangle + \frac{\mu}{3} \boldsymbol{\nabla} \left(\boldsymbol{\nabla} \cdot \langle \boldsymbol{v}_2 \rangle \right)$$
$$- \tau \boldsymbol{\nabla} \cdot \langle \boldsymbol{v}_1 \cdot \boldsymbol{\nabla} \boldsymbol{\sigma}_1^{ve} \rangle + \tau \boldsymbol{\nabla} \cdot \langle (\boldsymbol{\nabla} \boldsymbol{v}_1)^T \cdot \boldsymbol{\sigma}_1^{ve} \rangle + \tau \boldsymbol{\nabla} \cdot \langle \boldsymbol{\sigma}_1^{ve} \cdot \boldsymbol{\nabla} \boldsymbol{v}_1 \rangle . \tag{1.11}$$

In case of viscoelastic fluid acoustic radiation force can be expressed as

$$\boldsymbol{F}_{rad} = \left\langle \oint_{\partial s} (\boldsymbol{\sigma}_2 - \rho_0 \boldsymbol{v}_1 \boldsymbol{v}_1) \cdot \boldsymbol{n} dA \right\rangle . \tag{1.12}$$

Where the time-averaged second-order stress tensor is represented as

$$\langle \boldsymbol{\sigma}_2 \rangle = - \langle p_2 \rangle \boldsymbol{I} + \mu \left[\boldsymbol{\nabla} \langle \boldsymbol{v}_1 \rangle + (\boldsymbol{\nabla} \langle \boldsymbol{v}_1 \rangle)^T - \frac{2}{3} \left(\boldsymbol{\nabla} \cdot \langle \boldsymbol{v}_1 \rangle \right) \boldsymbol{I} \right] - \tau \langle \boldsymbol{v}_1 \cdot \boldsymbol{\nabla} \boldsymbol{\sigma}_1^{ve} \rangle$$
$$+ \tau \left\langle (\boldsymbol{\nabla} \boldsymbol{v}_1)^T \cdot \boldsymbol{\sigma}_1^{ve} \right\rangle + \tau \left\langle \boldsymbol{\sigma}_1^{ve} \cdot \boldsymbol{\nabla} \boldsymbol{v}_1 \right\rangle . \tag{1.13}$$

The first-order viscoelastic stress tensor can be expressed as

$$\boldsymbol{\sigma}_1^{ve} = \frac{\mu_p}{1 + i\omega\tau} \left[\boldsymbol{\nabla} \boldsymbol{v}_1 + (\boldsymbol{\nabla} \boldsymbol{v}_1)^T - \frac{2}{3} \left(\boldsymbol{\nabla} \cdot \boldsymbol{v}_1 \right) \boldsymbol{I} \right] . \tag{1.14}$$

In Figure 2 of main file, applying far field inviscid condition, $\mu = 0$ ($\mu_s = 0, \mu_p = 0$) gives $\boldsymbol{\sigma}_1^{ve} = 0$, equations (1.11) and (1.13) reduces to

$$\langle \rho_1 \partial_t \boldsymbol{v}_1 \rangle + \rho_0 \langle \boldsymbol{v}_1 \cdot \boldsymbol{\nabla} \boldsymbol{v}_1 \rangle = -\boldsymbol{\nabla} \langle p_2 \rangle \tag{1.15}$$

and

$$\langle \boldsymbol{\sigma}_2 \rangle = - \langle p_2 \rangle \boldsymbol{I} . \tag{1.16}$$

Substituting equation (1.16) in equation (1.12) and rearranging gives

$$\boldsymbol{F}_{rad} = - \int_s dA \left\{ \langle p_2 \rangle \boldsymbol{n} + \rho_0 \langle (\boldsymbol{n} \cdot \boldsymbol{v}_1) \boldsymbol{v}_1 \rangle \right\} . \tag{1.17}$$

Considering $\mu = 0$, equation (1.2) reduces to

$$\rho_0 \partial_t v_1 = -\boldsymbol{\nabla} p_1 . \tag{1.18}$$

Substituting (1.15) in (1.17) and simplifying using (1.18) and $p_1 = \rho_1 c_0^2$ gives

$$\boldsymbol{F}_{rad} = - \int_s dA \left\{ \left[\frac{\kappa_0}{2} \langle p_1^2 \rangle - \frac{\rho_0}{2} \langle v_1^2 \rangle \right] \boldsymbol{n} + \rho_0 \langle (\boldsymbol{n} \cdot \boldsymbol{v}_1) \boldsymbol{v}_1 \rangle \right\} . \tag{1.19}$$

Here, (1.19) is same as Settnes & Bruus (2012). By following the similar analogy we obtain an expression for F_{rad},

$$\boldsymbol{F}_{rad} = -\boldsymbol{\nabla} U_{rad}, \tag{1.20}$$

where

$$U_{rad} = \frac{4\pi}{3} a^3 \left[f_1 \frac{\kappa_0}{2} \langle p_{in}^2 \rangle - f_2 \frac{3\rho_0}{4} \langle v_{in}^2 \rangle \right] . \tag{1.21}$$

A detailed derivation of (1.20), (1.21) from (1.19) is reported in Bruus (2012) and Settnes & Bruus (2012). For a standing wave (1.21) becomes

$$U_{\text{rad}} = \frac{4\pi}{3}a^3\left[f_1^r\frac{\kappa_0}{2}\left\langle p_{in}^2\right\rangle - f_2^r\frac{3\rho_0}{4}\left\langle v_{in}^2\right\rangle\right]. \tag{1.22}$$

where f_1^r and f_2^r are real part of f_1 and f_2 respectively.

1.3. *Calculation of scattering coefficients in viscoelastic fluid*

In the far-field (see Figure 2 of main file), the total scattering field ϕ_{sc}, which is given by $\phi_{sc} \approx \phi_{mp} + \phi_{dp}$, becomes

$$\phi_{sc}(r,t) = -f_1\frac{a^3}{3\rho_0}\frac{\partial_t\rho_{in}\left(t - r/c_0\right)}{r} - f_2\frac{a^3}{2}\boldsymbol{\nabla}\cdot\left[\frac{\boldsymbol{v}_{in}\left(t - r/c_0\right)}{r}\right]. \tag{1.23}$$

where f_1 is the coefficient of monopole scattering potential and f_2 is the coefficient of dipole scattering potential. The monopole and dipole components have the form

$$\phi_{mp}(r) = -f_1\frac{a^3}{3\rho_0}\partial_t\rho_{in}\frac{1}{r}, \tag{1.24}$$

$$\phi_{dp}(r,\theta) = f_2\frac{a^3}{2}v_{in}\frac{\cos\theta}{r^2}, \tag{1.25}$$

and thus, total scattered field becomes

$$\phi_{sc}(r,\theta) = -f_1\frac{a^3}{3\rho_0}\partial_t\rho_{in}\frac{1}{r} + f_2\frac{a^3}{2}v_{in}\frac{\cos\theta}{r^2}. \tag{1.26}$$

The first-order velocity field is given by,

$$\boldsymbol{v}_1 = \boldsymbol{\nabla}\phi_1 \tag{1.27}$$

and first-order pressure field can be expressed as

$$p_1 = -\rho_0\partial_t\phi_1 = -i\rho_0\omega\left(\phi_{in} + \phi_{sc}\right). \tag{1.28}$$

From the incoming and far-field scattered fields, we obtain an expression for the acoustic radiation force (refer § 1.2), which can be simplified as follows

$$\boldsymbol{F}_{rad} = -\boldsymbol{\nabla}U_{rad}. \tag{1.29}$$

Where U_{rad} is the acoustic potential,

$$U_{\text{rad}} = \frac{4\pi}{3}a^3\left[f_1\frac{\kappa_0}{2}\left\langle p_{in}^2\right\rangle - f_2\frac{3\rho_0}{4}\left\langle v_{in}^2\right\rangle\right]. \tag{1.30}$$

In equation (1.30), f_1 and f_2 are unknowns that need to be determined (Bruus 2012; Settnes & Bruus 2012) to predict the acoustic radiation force. We consider the instantaneous velocity of the particle, $\boldsymbol{V}_P$, with the particle traveling along the polar axis of the spherical polar coordinate system. The velocity variations depend only on r and θ due to the azimuthal symmetry of the problem and can be represented as

$$\boldsymbol{v} = v_r\boldsymbol{e}_r + v_\theta\boldsymbol{e}_\theta. \tag{1.31}$$

Moreover, the polar axis $\boldsymbol{e}_z$ and incoming waves are in the same direction, so $\boldsymbol{v}_{in}$ can be represented as $\boldsymbol{v}_{in} = v_{in}\boldsymbol{e}_z$. The incoming wave and particle velocity can be represented as,

$$\boldsymbol{v}_{in} = v_{in}\boldsymbol{e}_z = \cos\theta\ v_{in}\boldsymbol{e}_r - \sin\theta\ v_{in}\boldsymbol{e}_\theta \tag{1.32}$$

and

$$\boldsymbol{V}_P = V_P \boldsymbol{e}_z = \cos\theta \; V_P \boldsymbol{e}_r - \sin\theta \; V_p \boldsymbol{e}_\theta. \tag{1.33}$$

If a viscoelastic fluid containing a particle is exposed to pressure oscillations, the particle goes through compression and expansion, resembling the behaviour of the fluid. When the compressibility of the particle is different from that of the fluid, the particle will encounter a more or less contraction and expansion than the fluid (Challis *et al.* 2005). Such a divergence may give rise to a fluid flow towards or away from the particle depending upon the compressibility contrast. Earlier studies (Challis *et al.* 2005; Bruus 2012) have reported that a particle could act as a sound emitter, emitting sound waves at the same frequency as that of the incident compression wave but potentially at a different phase.

If the particle is considerably smaller than the sound wavelength and has a spherical shape, the local field around the particle will resemble that of a basic monopole source (Bruus 2012; Settnes & Bruus 2012; Karlsen & Bruus 2015), shown in Figure 2(*b*). If the particle compressibility is more than that of the surrounding viscoelastic fluid, the compressible particle will cause fluid ejection at a rate of $\partial_t m$. The ejected mass can be evaluated by using the scattered first order velocity field, $\rho\boldsymbol{v}_{sc}$. To get the total volume ejection around the particle, $\rho\boldsymbol{v}_{sc}$ is calculated through a surface ∂s around the particle in the near field region.

The total fluid ejection caused by the particle is given by

$$\partial_t m = \oint_{\partial s} dA \boldsymbol{e}_r \cdot (\rho_0 \boldsymbol{v}_{sc}) = \oint_{\partial s} dA \boldsymbol{e}_r \cdot (\rho_0 \boldsymbol{\nabla}\phi_{mp}) = f_1 \frac{4\pi}{3} a^3 \partial_t \rho_{in}. \tag{1.34}$$

The ejected mass can be expressed in terms of incoming density and particle velocity as,

$$\partial_t m = \partial_t \left[(\rho_0 + \rho_{in}) V_P \right]. \tag{1.35}$$

Where V_P is the particle volume. By modifying equation (1.35) using compressibility $\kappa = -(1/V)(\partial V/\partial p)$, and introducing particle compressibility κ_P and viscoelastic fluid compressibility $\kappa_0 = 1/(\rho_0 c_0^2)$, we obtain

$$\partial_t m = \left[1 - \frac{\kappa_P}{\kappa_0} \right] V_P \partial_t \rho_{in}. \tag{1.36}$$

Comparing equations (1.34) and (1.36), we obtain monopole scattering coefficient expression as

$$f_1(\kappa_P^*) = 1 - \kappa_P^*. \tag{1.37}$$

Where compressibility ratio, $\kappa_P^* = \kappa_P/\kappa_0$. The expression for f_1 in a viscoelastic fluid is similar to that obtained for ideal and viscous fluids (Gorkov 1962; Bruus 2012; Settnes & Bruus 2012). This is due to the fact that the viscous and elastic properties (μ and τ) of the fluid do not impact mass ejection and f_1 only depends upon the compressibility ratio of the particle to viscoelastic fluid. When $\kappa_P = \kappa_0$, f_1 becomes zero and the expansion and contraction of fluid and particle become same leading to disappearing monopole scattering.

The viscoelastic properties of the fluid will have a significant effect on the dipole scattering coefficient, f_2 that arises due to the density difference between a particle and the suspending fluid (Bruus 2012). When a particle is denser than the surrounding fluid, pressure waves undergo cyclic variations in pressure gradient. This variation causes the particle to undergo oscillatory motion due to differences in inertia between the particle and the fluid (Challis *et al.* 2005). Previous studies have indicated that particle movement in a fluid is influenced by the formation of a viscous boundary layer close to the particle's

surface in a viscous fluid (Settnes & Bruus 2012) and by the formation of a viscous and thermal boundary layer in a thermoviscous fluid (Karlsen & Bruus 2015). Consequently, the expression for f_2, which is a measure of the scattering effect gets modified and there is a change in the acoustic radiation force, to account for the viscous and thermoviscous effects.

Here, we develop a modified expression for f_2 considering the viscous as well as elastic effects of a viscoelastic fluid. The basic equation forming the starting point for our theory for f_2 is the first-order Navier-Stokes equation (1.2). Here, we derive the first-order velocity and pressure, $\boldsymbol{v}_{ab}$ and p_{ab}, explicitly from equation (1.2) in the boundary layer region $a < r \lesssim a + 5\delta_{ve}$. As discussed earlier, in the boundary layer region, the fluid is considered incompressible, implying $\boldsymbol{\nabla} \cdot \boldsymbol{v}_{ab} = 0$. Taking divergence, equation (1.2) can be expressed as,

$$\nabla^2 p_{ab} = 0. \tag{1.38}$$

Moreover, considering the dipole part of the solution in ϕ_{sc}, we modify equation (1.28) as

$$p_{ab} = -i\rho_0\omega \left(\phi_{in} + \phi_{dp} \right). \tag{1.39}$$

Using equations (1.25) and (1.27) in equation (1.39), we obtain

$$p_{ab}(r, \theta) = -i\rho_0\omega \left[r + \frac{1}{2}\frac{a^3}{r^2}f_2 \right] v_{in} \cos\theta. \tag{1.40}$$

At the surface of particle $(r = a)$, the pressure field becomes

$$p_{ab}(a, \theta) = -i\rho_0\omega a \left[1 + \frac{1}{2}f_2 \right] v_{in} \cos\theta. \tag{1.41}$$

We derive $\boldsymbol{v}_{ab}$ from the first order Navier-Stokes equation (1.2), by combining the incompressibility and azimuthal symmetry. We introduce stream function $\psi(r, \theta)$ to express the velocity components inside the boundary layer region that helps to replace the vector equation for $\boldsymbol{v}_{ab}$ with a scalar equation for ψ as follows,

$$\boldsymbol{v}_{ab}(r, \theta) = \boldsymbol{\nabla} \times \left[\psi(r, \theta)\boldsymbol{e}_\varphi \right]. \tag{1.42}$$

Taking curl of equation (1.2) and upon simplification, we get

$$\rho_0 \boldsymbol{\nabla} \times (\partial_t \boldsymbol{v}_{ab}) = \mu_c \nabla^2 \left(\boldsymbol{\nabla} \times \boldsymbol{v}_{ab} \right). \tag{1.43}$$

Substituting $\partial_t \boldsymbol{v}_{ab} = i\omega \boldsymbol{v}_{ab}$ and equation (1.42) in equation (1.43) yields

$$i\rho_0\omega \nabla^2 \left(\psi(r, \theta)\boldsymbol{e}_\varphi \right) = \mu_c \nabla^2 \nabla^2 \left(\psi(r, \theta)\boldsymbol{e}_\varphi \right). \tag{1.44}$$

Upon simplification of equation (1.44), we obtain

$$\nabla^2 \left(\nabla^2 - \frac{i\rho_0\omega}{\mu_c} \right) \left[\psi(r, \theta)\boldsymbol{e}_\varphi \right] = 0 \tag{1.45}$$

To study the effect of viscoelastic parameters, we collect the complex viscosity term from equation (1.45) and represented as

$$q_{ve} = \sqrt{-\frac{i\rho_0\omega}{\mu_c}}. \tag{1.46}$$

By using equation (1.46), equation (1.45) reduces to

$$\nabla^2 \left(\nabla^2 + q_{ve}^2 \right) \left[\psi(r, \theta)\boldsymbol{e}_\varphi \right] = 0. \tag{1.47}$$

Considering the expression for δ_{ve} (equation 2.20 of main file) and λ_{ve} (equation 2.21 of main file), equation (1.46) can be written as follows,

$$q_{ve} = \frac{(1-i)}{2} \left[\left(\frac{1}{\delta_{ve}} + \frac{2\pi}{\lambda_{ve}} \right) - i \left(\frac{1}{\delta_{ve}} - \frac{2\pi}{\lambda_{ve}} \right) \right]. \tag{1.48}$$

For a viscous fluid, $\lambda_{ve}/\delta_{ve} = \lambda_v/\delta_v = 2\pi$ (Doinikov *et al.* 2021*a*). Hence, in the absence of elasticity, equation (1.48) reduces to $q_{ve} = q_v = (1-i)/\delta$.

If $q_{ve} \neq 1$, the differential operators in equation (1.47) are different. Therefore, we introduce $\psi(r,\theta) = \psi_1(r,\theta) + \psi_2(r,\theta)$ in equation (1.47), obtaining

$$\nabla^2 \left(\nabla^2 + q_{ve}^2 \right) \left[(\psi_1(r,\theta) + \psi_2(r,\theta)) \, \boldsymbol{e}_\varphi \right] = 0. \tag{1.49}$$

Where ψ_1 and ψ_2 satisfies

$$\nabla^2 \left[\psi_1(r,\theta) \boldsymbol{e}_\varphi \right] = 0 \tag{1.50}$$

and

$$\left(\nabla^2 + q_{ve}^2 \right) \left[\psi_2(r,\theta) \boldsymbol{e}_\varphi \right] = 0. \tag{1.51}$$

The stream function only depends on (r,θ), therefore

$$\boldsymbol{\nabla}^2 \left[\psi(r,\theta) \boldsymbol{e}_\varphi \right] = \left[\nabla^2 \psi - \frac{\psi}{(r\sin\theta)^2} \right] \boldsymbol{e}_\varphi. \tag{1.52}$$

Using equation (1.52), we expand equations (1.50) and (1.51) as

$$\nabla^2 \psi_1 - \frac{\psi_1}{(r\sin\theta)^2} = 0 \tag{1.53}$$

and

$$\nabla^2 \psi_2 - \frac{\psi_2}{(r\sin\theta)^2} = -q_{ve}^2 \psi_2. \tag{1.54}$$

Solution of equation (1.53) can be expressed in Legendre form,

$$\psi_1(r,\theta) = A_1 r \cos\theta + \frac{A_2 \cos\theta}{r^2}. \tag{1.55}$$

Where A_1 and A_2 are unknowns. However, solution of (1.54) depends upon q_{ve} and can be expressed in Hankel form,

$$\psi_2(r,\theta) = B h_1^1(q_{ve}r) a v_{in} \sin\theta. \tag{1.56}$$

Here, $h_1^1(q_{ve}r)$ is the spherical Hankel function of first kind of order 1, $h_1^1(q_{ve}r) = -e^{iq_{ve}r}(q_{ve}r+i)/(q_{ve}r)^2$. Substituting q_{ve} from equation (1.48) in Hankel function shows a decaying variation of ψ_2 with the length scale. Here, $h_1^1(q_{ve}r) \propto e^{iq_{ve}r}$. By substituting the expression for q_{ve} and further simplification gives $h_1^1(q_{ve}r) \propto e^{-r/\delta_{ve}}$. Therefore, with an increasing the r spherical Hankel function $h_1^1(q_{ve}r)$ decreases and becomes less than 1% for $r \approx 4.6\delta_{ve}$. The exact value of the prefactor is not critical to our analysis. Therefore we consider $5\delta_{ve}$ to define the near field region. Furthermore, B is an unknown and A_1, A_2 and B need to be determined to get the first order scattering field inside the boundary layer region.

We determine the values of A_1 and A_2 in equation (1.55) by asymptotic matching of velocity field in boundary layer region with dipole part of fluid velocity in near field region, $\boldsymbol{v}_{ab}(r \approx r^*,\theta) = \boldsymbol{\nabla} \times \left[\psi_1 \boldsymbol{e}_\varphi \right]$ (Settnes & Bruus 2012). Using equations (1.25), (1.27) and (1.32), fluid velocity in the near field region can be written as

$$\boldsymbol{v}_{ab}(r \approx r^*,\theta) = \left[1 - f_2 \frac{a^3}{r^3} \right] \cos\theta \, v_{in} \cdot \boldsymbol{e}_r + \left[1 + \frac{1}{2} f_2 \frac{a^3}{r^3} \right] (-\sin\theta) \, v_{in} \cdot \boldsymbol{e}_\theta. \tag{1.57}$$

Comparing equation (1.57) with $\boldsymbol{\nabla} \times \left[\psi_1 e_\varphi \right]$ gives

$$\psi_1(r, \theta) = \left[\frac{1}{2} r - \frac{f_2}{2} \frac{a^3}{r^2} \right] \sin \theta \; v_{in}. \tag{1.58}$$

The next step is to represent the velocity field inside the boundary layer using equations (1.58) and (1.56), $v_{ab} = \boldsymbol{\nabla} \times \left[(\psi_1 + \psi_2) \, e_\varphi \right]$, a simplified expression for v_{ab} is as follows,

$$\boldsymbol{v}_{ab} \cdot \boldsymbol{e}_r = \left[1 - f_2 \frac{a^3}{r^3} + 2q_{ve}aB \left(\frac{h_1^1(s)}{s} \right)_{q_{ve}r} \right] \cos \theta \; v_{in} \tag{1.59}$$

and

$$\boldsymbol{v}_{ab} \cdot \boldsymbol{e}_\theta = \left[1 + \frac{f_2}{2} \frac{a^3}{r^3} + q_{ve}aB \left\{ \frac{\partial_s \left(s h_1^1(s) \right)}{s} \right\}_{q_{ve}r} \right] (-\sin \theta) \; v_{in}. \tag{1.60}$$

Furthermore, we determine the value of B by considering no-slip condition at the surface of particle ($r = a$). The associated boundary conditions can be written as

$$\boldsymbol{v}_{ab}(a, \theta) \cdot \boldsymbol{e}_r = \cos \theta \; V_P \tag{1.61}$$

and

$$\boldsymbol{v}_{ab}(a, \theta) \cdot \boldsymbol{e}_\theta = (-\sin \theta) \; V_P. \tag{1.62}$$

In the above equations, V_P is the particle velocity and it is also an unknown. Therefore f_2, B and V_P are the unknowns presented in (1.59), (1.60), (1.61) and (1.62). As the particle is freely suspended, the translational velocity of the particle comes from the force free condition. Thus, to determine the particle velocity, we consider Newton's second law of motion on the particle. The inertial force on the particle is calculated by $m\partial_t V_P = \rho_P (4/3)\pi a^3 i\omega V_P$. In the next step, we balance the inertial force with total force around the particle, which comes from pressure and viscoelastic stress,

$$\rho_P \frac{4}{3} \pi a^3 i\omega V_P = \int_{\partial V} dA \; \boldsymbol{n} \cdot \boldsymbol{\sigma}_{ab} \cdot \boldsymbol{e}_z. \tag{1.63}$$

Considering pressure and viscoelastic stress, equation (1.63) can be modified as

$$\rho_P \frac{4}{3} \pi a^3 i\omega V_P = 2\pi a^2 \int_{-1}^{1} d(\cos \theta) \left[\left(-p_{ab} + \sigma_{rr}^{ab} \right) \cos \theta - \sigma_{\theta r}^{ab} \sin \theta \right]. \tag{1.64}$$

Here, the viscoelastic stress components are $\sigma_{rr}^{ab} = 2\mu_c \partial_r v_r^{ab}$ and $\sigma_{\theta r}^{ab} = \mu_c \left[r \partial_r \left(v_\theta^{ab}/r \right) + (1/r)\partial_\theta v_r^{ab} \right]$. We consider equations (1.59), (1.60) and apply no-slip boundary conditions at $r = a$ (see equations (1.61) and (1.62)) to obtain

$$V_P = \left[1 - f_2 + 2Bh_1^1(q_{ve}a) \right] v_{in} \tag{1.65}$$

and

$$V_P = \left[1 + \frac{1}{2} f_2 + B\partial_s \left(sh_1^1(s) \right)_{q_{ve}a} \right] v_{in}. \tag{1.66}$$

Substituting equations (1.41), (1.59), and (1.60) in σ_{rr}^{ab} and $\sigma_{\theta r}^{ab}$. Further simplification of (1.64) yields (Settnes & Bruus 2012)

$$\rho_P^* V_P = \left[1 + \frac{1}{2} f_2 + 2Bh_1^1(q_{ve}a) \right] v_{in}. \tag{1.67}$$

Here, $\rho_P^* = \rho_P/\rho_0$. Solving equations (1.65), (1.66) and (1.67), we obtain values of f_2, B

and V_p. Subtraction of equation (1.65) from equation (1.66) and substituting $\partial_s \left(sh_1^1(s)\right) = sh_0^1(s) - 3h_1^1(s)$, we get a relationship between f_2 and B.

Now, we consider following dimensionless variables

$$\delta_{ve}^* = \frac{\delta_{ve}}{a}, \quad \lambda_{ve}^* = \frac{\lambda_{ve}}{a} \tag{1.68}$$

and introduce

$$\gamma^* = \frac{3h_1^1(s)}{sh_0^1(s)}. \tag{1.69}$$

Where, $s = q_{ve}a$. Substituting equation (1.48) in equation (1.69) and expanding the expression, we get

$$\gamma^* \left(\delta_{ve}^*, \lambda_{ve}^*\right) = \frac{3(1+i)\left[1 + Q + i(1+P)\right]}{(P - iQ)^2}, \tag{1.70}$$

where,

$$P = \frac{1}{\delta_{ve}^*} + \frac{2\pi}{\lambda_{ve}^*} \quad \text{and} \quad Q = \frac{1}{\delta_{ve}^*} - \frac{2\pi}{\lambda_{ve}^*}. \tag{1.71}$$

Accordingly, we solve equation (1.67) with equations (1.65) and (1.66) to obtain

$$f_2 \left(\rho_P^*, \delta_{ve}^*, \lambda_{ve}^*\right) = \frac{2\left[1 - \gamma^* \left(\delta_{ve}^*, \lambda_{ve}^*\right)\right]\left(\rho_P^* - 1\right)}{2\rho_P^* + 1 - 3\gamma^* \left(\delta_{ve}^*, \lambda_{ve}^*\right)}. \tag{1.72}$$

The contrast factor is

$$\Phi \left(\kappa_P^*, \rho_P^*, \delta_{ve}^*, \lambda_{ve}^*\right) = \frac{1}{3}f_1(\kappa_P^*) + \frac{1}{2}f_2^r \left(\rho_P^*, \delta_{ve}^*, \lambda_{ve}^*\right). \tag{1.73}$$

2. Numerical modelling

We use numerical simulation models to assess variations in acoustic fluid field perturbations, acoustic energy density, and to do a comparison with radiation force theory. To establish relative boundary conditions for the 2D numerical models of acoustic energy density (AED) and radiation force (ARF), we conduct simulations of the entire experimental acoustofluidic device using COMSOL Multiphysics 6.0 (Dual & Möller 2012; Dual & Schwarz 2012; Hahn *et al.* 2015), with the base fluid being DI water. In the experiments, the input to the device is voltage applied to the transducer. Similarly, in the full device model, we maintain the same voltage input (U_{pp} = 13.2 V) to the transducer and adhere to similar design conditions as in the experimental setup. The numerical model, along with the mesh arrangement, is depicted in Figure 1(*a*) and (*b*). Here, we consider the thermoviscous acoustic module to solve the first-order equations, with simulation parameters akin to those outlined in Muller & Bruus (2014). Upon actuating the transducer, we observe first-order pressure variations inside the channel, as illustrated in Figure 1(*c*). To maintain a similar range of pressure variations within the AED and ARF numerical models, we set the boundary conditions accordingly.

2.1. *Acoustic energy density (AED) model and validation*

We present a 2D model for calculating acoustic energy density in viscoelastic fluids, following the work by Muller & Bruus (2014). In this model, we consider the cross-section of the channel as the computational domain and solve the first and second-order perturbation equations, as depicted in Figure 2. The dimensions of the channel cross-section closely resemble those of the experimental device, within the channel, we consider the viscoelastic fluid. To ensure accurate computation, we employ a non-homogeneous
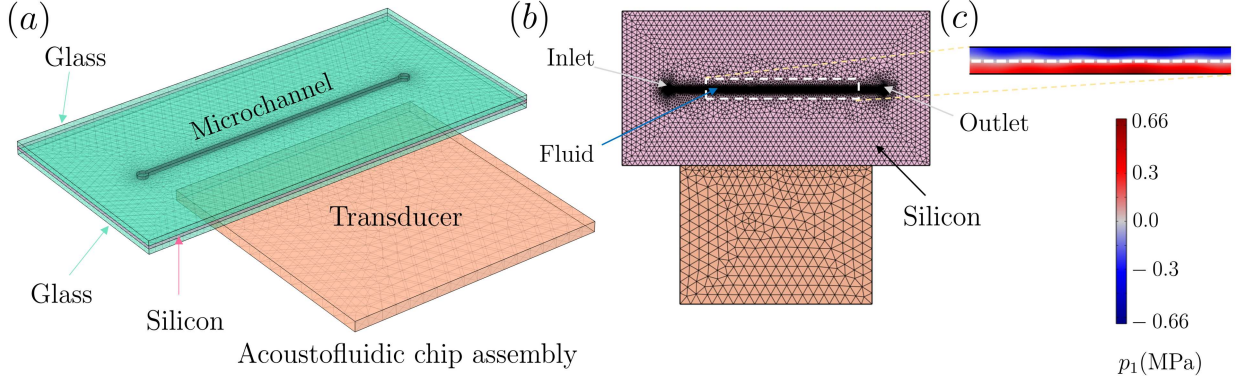
FIGURE 1. Numerical model for finding the first order pressure variation (*a*) 3D model of Glass-Si- Glass acoustofluidic device, illustrating the components and mesh distribution (*b*) 2D sectional view of the Silicon microchannel (*c*) variation of first order pressure field inside the channel for the base fluid (DI water). The nodal plane is indicated by white dashed lines.
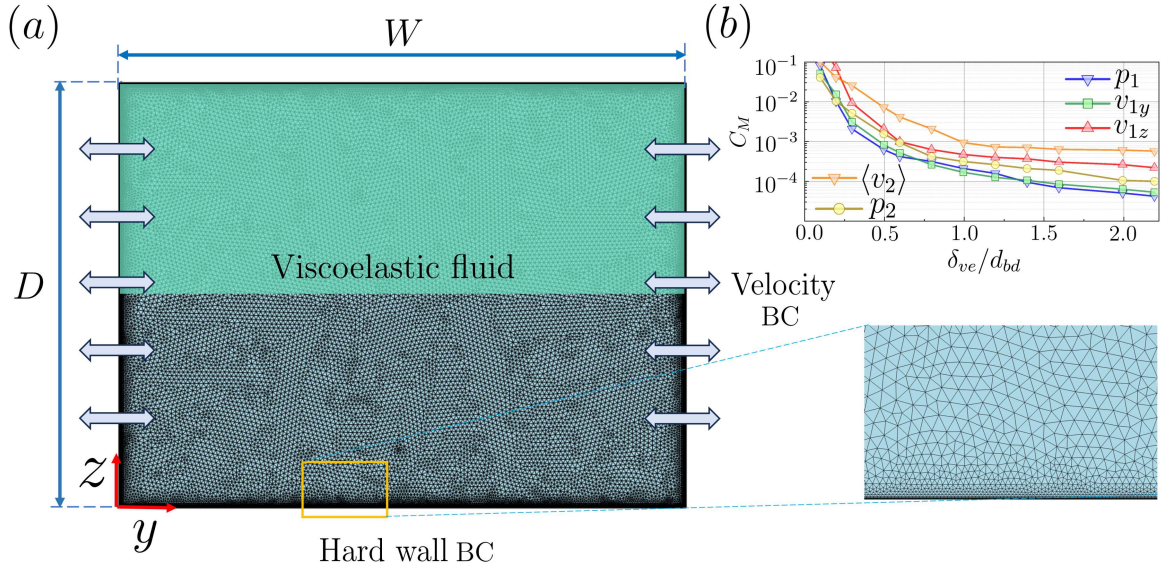

FIGURE 2. Numerical model for acoustic energy density calculation (*a*) 2D cross-section of channel with width W and depth D. The bottom half of the image depicts the mesh distribution. An enlarged view of the mesh distribution close to the wall is shown on the right side. The side walls are actuated by a velocity boundary condition, while the top and bottom walls are applied to a hard wall boundary condition. The axes x and y are considered at the bottom left corner of the cross-section. (*b*) Mesh convergence study for the domain, shows a semi-logarithmic plot oof the mesh convergence parameter C_M with the ratio of boundary layer thickness and mesh size in the boundary layer (δ_{ve}/d_{bd}).

mesh in the domain, with a very fine mesh near the acoustic boundary or close to the channel wall. The first-order perturbation equations are solved using the Thermoviscous acoustics module in COMSOL Multiphysics 6.0.

We apply the following boundary conditions to the channel walls, for top and bottom wall:

$$\hat{\boldsymbol{n}} \cdot \boldsymbol{v}_1 = 0. \tag{2.1}$$

For actuating side walls, the velocity boundary condition reduces to (Bach & Bruus 2018):

$$\boldsymbol{v}_1 = \boldsymbol{V}_1^0 (\boldsymbol{d}_0) = i\omega A \hat{e}_y. \tag{2.2}$$

Where $\boldsymbol{V}_1^0$ is the Lagrangian velocity of the wall, A and ω are the amplitude and angular
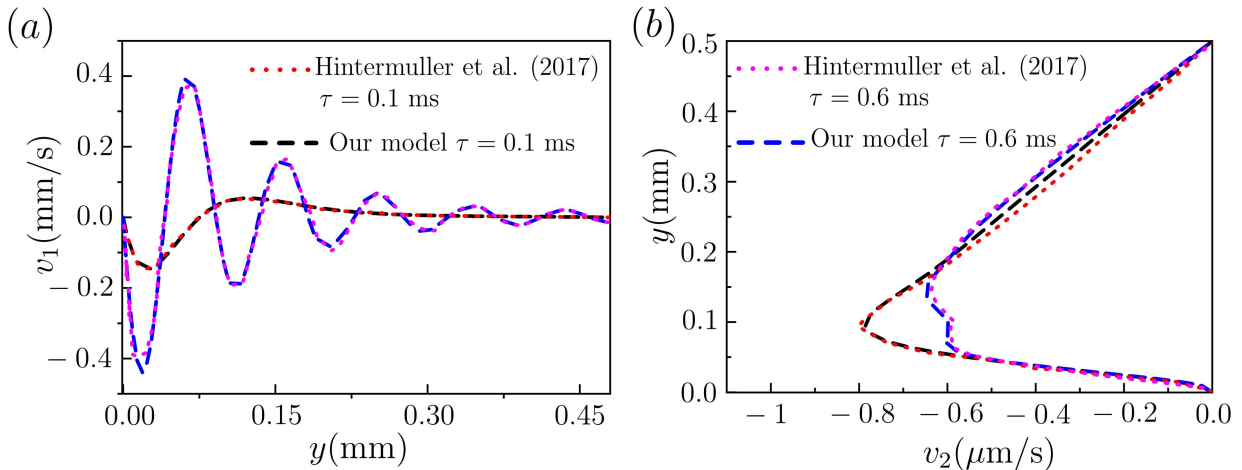
(*a*)

(*b*)

FIGURE 3. Validation of acoustic energy density model with Hintermuller *et al.* (2017), the comparison is done at $\tau = 0.1$ ms and 0.6 ms for (*a*) First order field (*b*) Time averaged second order velocity field.

frequency of vibration, respectively. We solve the second order perturbation equations using Laminar flow module with the extra viscoelastic stress terms, where following boundary conditions are considered.

For top and bottom wall: Lagrangian no-slip boundary condition gives,

$$\hat{\boldsymbol{n}} \cdot \boldsymbol{v}_2 = 0. \tag{2.3}$$

For actuating side walls:

$$\boldsymbol{v}_2 = -\langle (\boldsymbol{d}_1 \cdot \boldsymbol{\nabla}) \, \boldsymbol{v}_1 \rangle \tag{2.4}$$

Where, $\boldsymbol{d}_1 = \boldsymbol{u}_1/i\omega$, $\boldsymbol{n}$ is the normal vector to the surface and (2.4) is known as the Stokes drift.

A mesh convergence study is conducted following the approach outlined by Muller & Bruus (2014). We illustrate the variation of the mesh convergence parameter, C_M, with the ratio of the acoustic boundary layer thickness to the mesh size in the boundary layer (δ_{ve}/d_{bd}). The mesh convergence parameter, C_M, for a solution g with respect to a reference solution g_{ref}, is defined as

$$C_M(g) = \sqrt{\frac{\int (g - g_{\text{ref}})^2 \, dydz}{\int (g_{\text{ref}})^2 \, dydz}}. \tag{2.5}$$

We choose $C_M = 10^{-3}$, and both the first and second-order fields converge when δ_{ve}/d_{bd} exceeds 1. Therefore, we select the mesh by ensuring δ_{ve}/d_{bd} is greater than 1. Furthermore, we validated our numerical model for both first and second-order fluid fields against the findings of Hintermuller *et al.* (2017). The comparison results, depicted in Figure 3, demonstrate a close agreement between our results and theirs.

2.2. *Acoustic radiation force model*

We compare the derived acoustic radiation force (ARF) theory with the numerical ARF model. Since the radiation force is obtained through surface integration of stress terms, we introduce an axi-symmetrical (about z axis) numerical model in COMSOL Multiphysics 6.0, resembling the theoretical model. The particle is positioned at the center of the domain surrounded by viscoelastic fluid, with a perfectly matched layer (PML) provided around the fluid domain. We employ a non-homogeneous mesh with boundary layer refinement, by following the approach by Baasch *et al.* (2019), shown
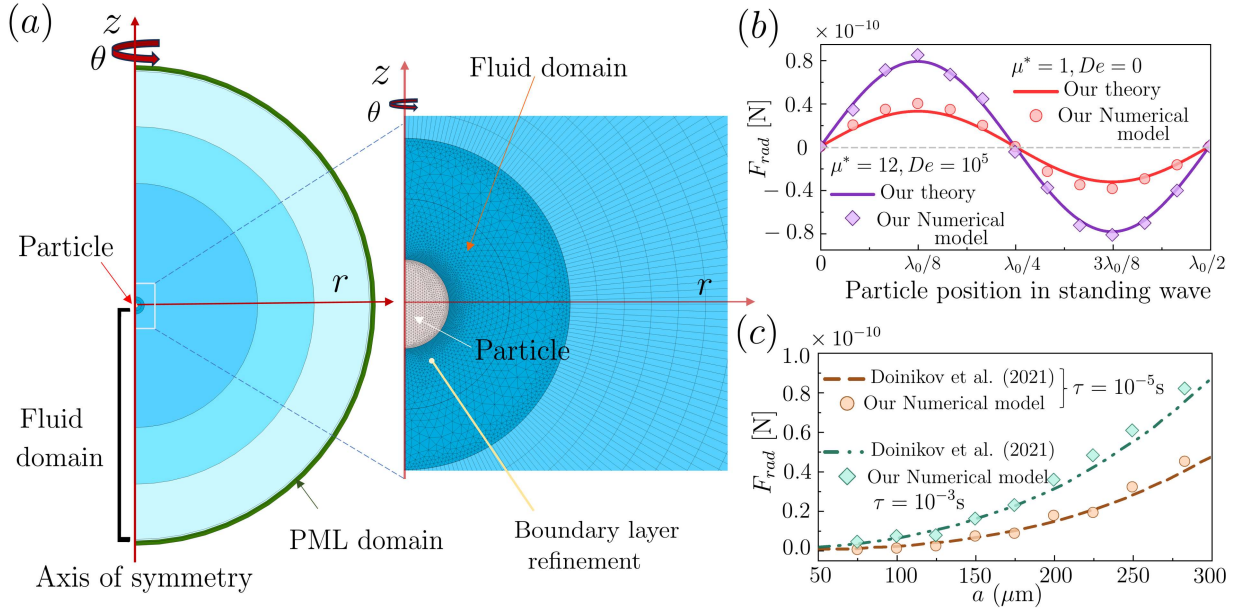
FIGURE 4. Numerical model for acoustic radiation force measurement in viscoelastic fluid (a) Computational domain is axi-symmetric about z axis of coordinate system (r, θ, z). The mesh distribution is shown on the right side. (b) Comparative study between our theory and numerical results on the distribution of ARF along standing wave direction. (c) Validation of numerical model with Doinikov *et al.* (2021*b*) for two cases of relaxation time $\tau = 10^{-3}$ and 10^{-5} s.

in Figure 4(*a*). The acoustic field is introduced by a background pressure field with a similar amplitude as in the Acoustic Energy Density (AED) model. We solve the first and second-order perturbation equations using the thermoviscous acoustics and laminar flow modules. The ARF is measured at different locations of the particle from one pressure anti-node to another. A comparison between the theoretical variation of ARF and ARF from the numerical model for two different cases is depicted in Figure 4(*b*), showing close agreement.

Additionally, we validate our numerical model with an existing study by Doinikov *et al.* (2021*b*), provided in Figure 4(*c*).

3. Experiments and details

3.1. *Viscoelastic fluid preparation and properties*

Polymer powder at different concentrations by wt.% are dissolved in deionized water by gentle mixing followed by sonication for 15 min. All solutions were kept on a mixing stage for 24 h to avoid precipitation and fully dissolve the polymer. Apart from PVP 0.36MDa, we additionally consider PEO 0.4MDa and 1MDa fluids in the experiments, and their properties are provided in Table 1. We measure the viscosity using Anton-Paar rheometer MCR 72 and calculate the relaxation times by following Tirtaatmadja *et al.* (2006); Ebagninin *et al.* (2009).

3.2. *Relaxation time measurement*

The relaxation time (τ) of a polymer solution or viscoelastic fluid depends on the concentration and molecular weight of the polymer. Polymer solutions are categorized based on concentration and molecular weight into dilute, semi-dilute unentangled, semi-dilute entangled, and concentrated solutions (Rouse 1953; Zimm 1956; Tirtaatmadja *et al.* 2006; Ebagninin *et al.* 2009). Critical concentrations (C^*, C^{**}), and entanglement concentration (C^e) are introduced in the literature to differentiate between the nature of

Solutions	C [wt.%]	μ [mPa s]	τ [s]	$\mu^* = \mu/\mu_{bf}$	$De = \tau\omega$
PEO (0.4 MDa)	2.50	66.7	6.1×10^{-3}	75.0	7.4×10^4
	3.50	180.7	2.1×10^{-2}	203.0	2.5×10^5
PEO (1 MDa)	0.74	18.9	3.0×10^{-3}	21.3	3.7×10^4
	1.05	40.1	4.7×10^{-3}	45.1	5.7×10^4
	1.40	61.8	1.4×10^{-2}	69.5	1.7×10^5

TABLE 1. Fluid concentration and viscoelastic properties (Rouse 1953; Zimm 1956; Tirtaatmadja *et al.* 2006; Ebagninin *et al.* 2009)

these solutions. In dilute polymer solutions, the elastic properties may not be accurately captured using Rheometers, as the relaxation time varies beyond the sensitivity of the instrument. Zimm (1956) formulated the relaxation time of dilute solutions as

$$\lambda_z \cong \frac{F[\eta]M_w\eta_s}{RT}, \tag{3.1}$$

$$[\eta] = 0.072M_w^{0.65} \quad C^* = \frac{1}{[\eta]}. \tag{3.2}$$

Here, for good solvents like water $F = 0.463$, $[\eta]$ is intrinsic viscosity, M_w is the molecular weight of the polymer, η_s solvent viscosity, R universal gas constant, T is the absolute temperature. The effect of concentration on relaxation time was considered by Tirtaatmadja *et al.* (2006), reported an effective relaxation time,

$$\lambda_{eff} \cong \frac{F[\eta]M_w\eta_s}{RT}\left(\frac{C}{C^*}\right)^{0.65} \quad 0.01 \leqslant C/C^* \leqslant 1. \tag{3.3}$$

The relaxation time of various dilute polymer solutions reported in this study is calculated using Equations (3.1) and (3.3). The transition of polymer solutions from dilute to semi-dilute unentangled regime causes the rate of increase in the viscoelastic properties with the concentration of polymer, which can be measured by rheometer and various other methods reported in the literature (Ebagninin *et al.* 2009). Most of the body fluids are having viscoelastic properties similar to the dilute and semi-dilute unentangled solutions, therefore our experiments are conducted for dilute and semi-dilute unentangled polymer solutions.

4. Results and discussion

4.1. *Contrast factor variation*

The total scattering is characterized by contrast factor (Φ), considering f_1 and f_2. The contrast factor is calculated from equation (1.73), which relies on the density (ρ_P^*) and compressibility (κ_P^*) ratio between particle and fluid, dimensionless acoustic boundary layer thickness and viscous wavelength. We represnts the relative change in contrast factor (Ω) of particles in a viscoelastic fluid compared to a ideal fluid is depicted in Figure 5. This change is represented by $\Omega = \left(\Phi\left(\kappa_P^*, \rho_P^*, \delta_{ve}^*, \lambda_{ve}^*\right) - \Phi(\kappa_P^*, \rho_P^*, 0, 0)\right)/\Phi(\kappa_P^*, \rho_P^*, 0, 0)$ in percentage. Specifically, for PS, MESC2.10 cell, MR, PM, silica, and pyrex particles in viscoelastic fluid with properties: $\mu_s^* = 1, \mu_P^* = 10, De = 200, \rho^* = 1.005$, and $c^* = 1$, Ω exhibits variations of up to 0.3%, 3.75%, 2.6%, 11.8%, 27%, and 39% respectively.
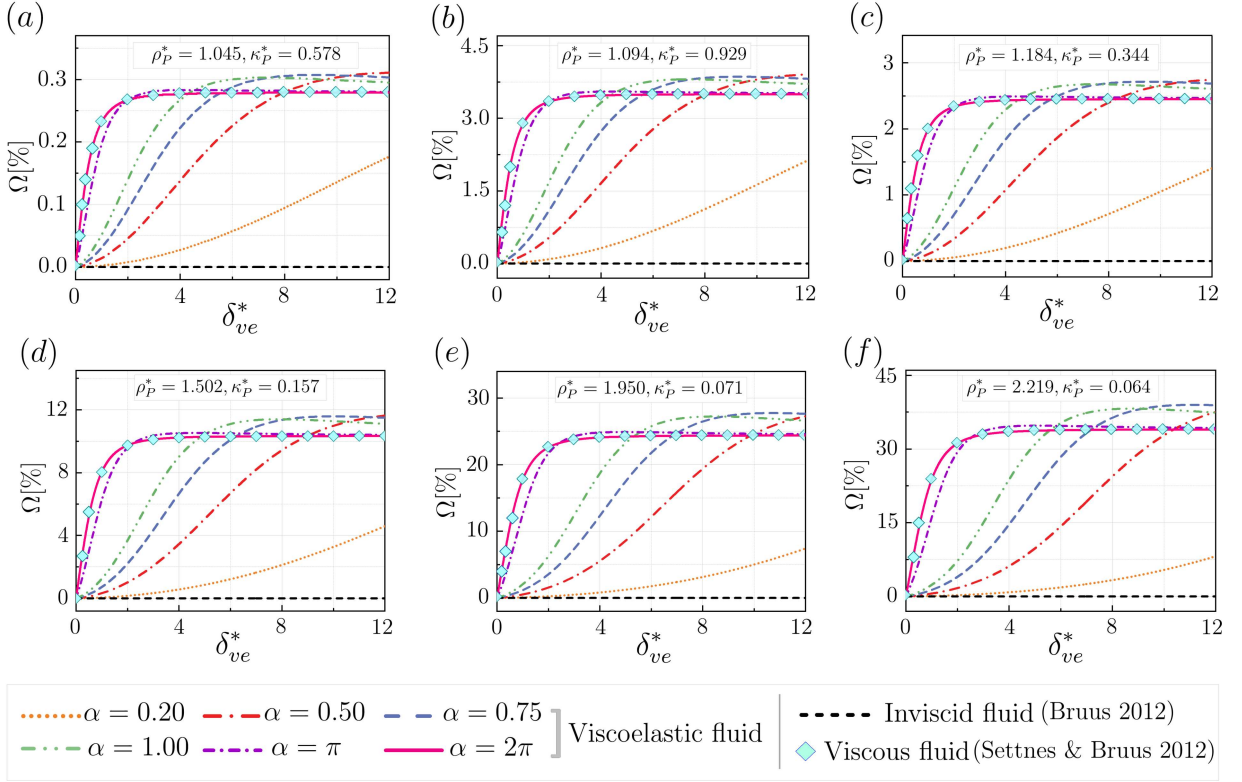
FIGURE 5. Theoretical variation of percentage change in relative contrast factor, $\Omega[\%]$, with δ_{ve}^* for (*a*) PS: $\rho_P^* = 1.045, \kappa_P^* = 0.578$ (*b*) MESC2.10 cell: $\rho_P^* = 1.094, \kappa_P^* = 0.929$ (*c*) PM: $\rho_P^* = 1.184, \kappa_P^* = 0.344$ (*d*) MR: $\rho_P^* = 1.502, \kappa_P^* = 0.157$ (*e*) Silica: $\rho_P^* = 1.950, \kappa_P^* = 0.071$ (*f*) Pyrex: $\rho_P^* = 2.219, \kappa_P^* = 0.064$ (Settnes & Bruus 2012). Particles are suspended in viscoelastic fluid with properties: $\mu_s^* = 1, \mu_p^* = 10, De = 200, \rho^* = 1.005,$ and $c^* = 1.$
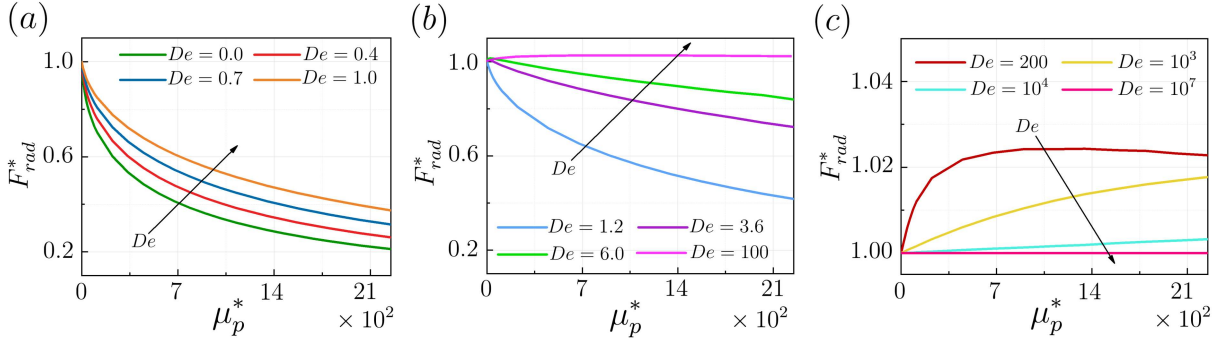

FIGURE 6. Variation of acoustic radiation force (F_{rad}^*) with μ_p^* at different De. (*a*) $De \leqslant 1$ (*b*) $1 < De \leqslant 100$ (*c*) $De > 100$. The arrow signifies the direction of increase in De and we consider $\mu_s^* = 1, \rho^* = 1, \rho_P^* = 1.05$ and $c^* = 1.$

4.2. *Acoustic radiation force variation*

We show the variation of F_{rad}^* with μ_p^* in Figure 6 for three cases: (*a*)$De \leqslant 1$, (*b*)$1 < De \leqslant 100$, and (*c*)$De \geqslant 200$. Here, F_{rad}^* follows the same trend of E_{ac}^* (Figure 5*a* of main file) due to the negligible effect of viscoelastic properties on ACF of Polystyrene particles. Similarly, F_{rad}^* variation with μ_s^*, in Figure 7 shows same trend as acoustic energy density variation as given in main file (Figure 6*a* of main file).
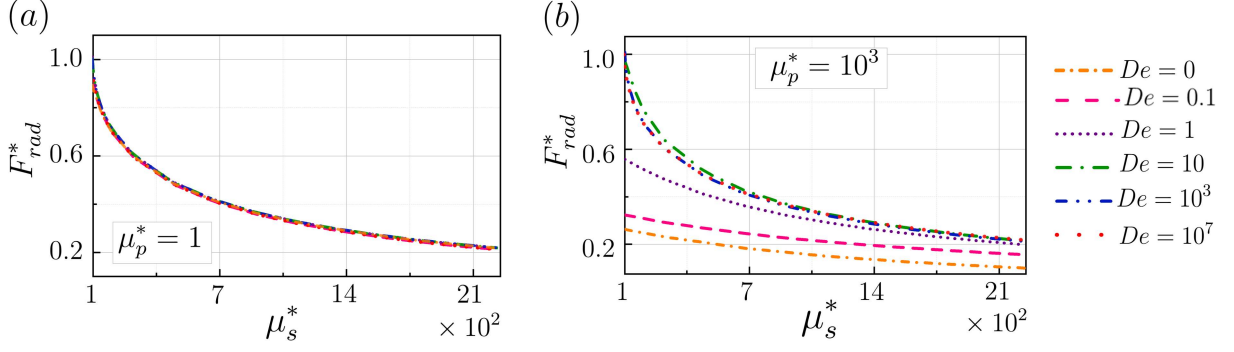
FIGURE 7. Variation of dimensionless acoustic radiation force (F_{rad}^*) with μ_s^* at different De $(0, 0.1, 1, 10, 10^3, 10^7)$ and (a) $\mu_p^* = 1$ (b) $\mu_p^* = 10^3$. Here we consider $\rho_P^* = 1.05$ $\rho^* = 1$ and $c^* = 1$.
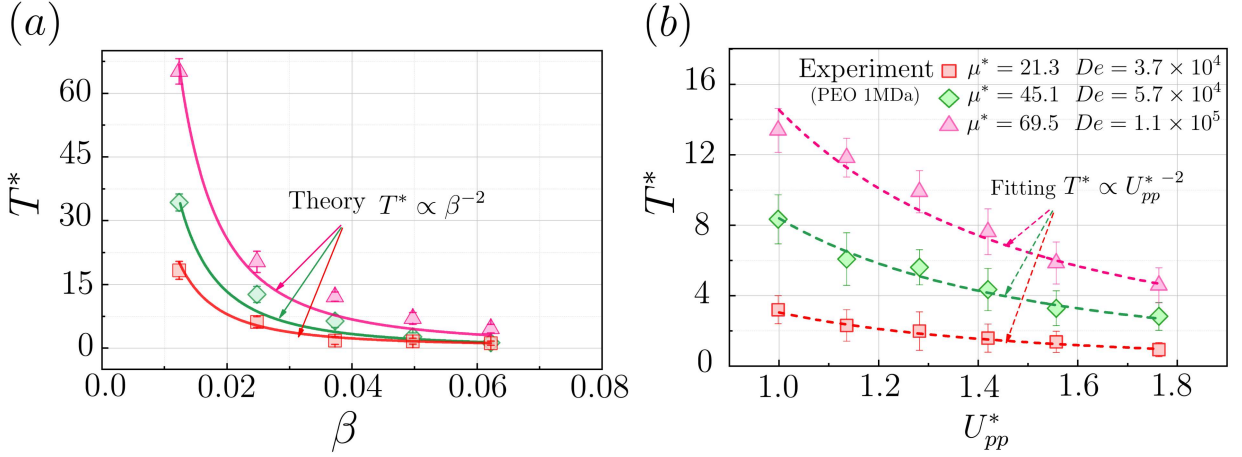

FIGURE 8. Experimental and theoretical variation of normalized acoustic particle central migration time (T^*) in PEO 1 MDa of $C = 0.74\%$ ($\mu^* = 21.3, De = 3.7 \times 10^4, \rho^* = 1.007, c^* = 1.003$), 1.05% ($\mu^* = 45.1$, $De = 5.7 \times 10^4$, $\rho^* = 1.015, c^* = 1.006$) and 1.4% ($\mu^* = 69.5, De = 1.7 \times 10^5$, $\rho^* = 1.020, c^* = 1.010$) with (a) blockage ratio (β) at $U_{pp}^* = 1.14$, where $T^* \propto \beta^{-2}$ (b) dimensionless peak-to-peak voltage (U_{pp}^*) at $\beta = 0.0375$, where, $T^* \propto U_{pp}^{*-2}$.

4.3. *Effect of Particle size and voltage input in particle migration*

The effect of particle size (β) and peak-to-peak voltage input (U_{pp}^*) to the transducer on particle migration in different viscoelastic fluids is illustrated in Figure 8. It is observed that the rate of decrease in T^* with β and U_{pp}^* is higher for larger μ^* and De. This is because the acoustic boundary layer thickness is greater for $\mu^* = 69.5, De = 1.7 \times 10^5$ due to the higher viscosity. At low voltage and for small particles, this boundary layer effect becomes dominant, and with an increase in β and U_{pp}^*, the boundary layer effects reduces at a faster rate.

REFERENCES

BAASCH, THIERRY, PAVLIC, ALEN & DUAL, JÜRG 2019 Acoustic radiation force acting on a heavy particle in a standing wave can be dominated by the acoustic microstreaming. *Physical Review E* **100** (6).

BACH, JACOB S. & BRUUS, HENRIK 2018 Theory of pressure acoustics with viscous boundary layers and streaming in curved elastic cavities. *The Journal of the Acoustical Society of America* **144** (2), 766–784.

BRUUS, HENRIK 2012 Acoustofluidics 7: The acoustic radiation force on small particles. *Lab on a Chip* **12** (6), 1014.

CHALLIS, R. E., POVEY, M. J.W., MATHER, M. L. & HOLMES, A. K. 2005 Ultrasound techniques for characterizing colloidal dispersions. *Reports on Progress in Physics* **68** (7), 1541–1637.

DOINIKOV, ALEXANDER A., FANKHAUSER, JONAS & DUAL, JÜRG 2021*a* Nonlinear dynamics of a solid particle in an acoustically excited viscoelastic fluid. i. acoustic streaming. *Physical Review E* **104** (6).

DOINIKOV, ALEXANDER A., FANKHAUSER, JONAS & DUAL, JÜRG 2021*b* Nonlinear dynamics of a solid particle in an acoustically excited viscoelastic fluid. ii. acoustic radiation force. *Physical Review E* **104** (6).

DUAL, JURG & MÖLLER, DIRK 2012 Acoustofluidics 4: Piezoelectricity and application in the excitation of acoustic fields for ultrasonic particle manipulation. *Lab on a Chip* **12** (3), 506.

DUAL, JURG & SCHWARZ, THOMAS 2012 Acoustofluidics 3: Continuum mechanics for ultrasonic particle manipulation. *Lab Chip* **12** (2), 244–252.

EBAGNININ, KOBLAN WILFRIED, BENCHABANE, ADEL & BEKKOUR, KARIM 2009 Rheological characterization of poly(ethylene oxide) solutions of different molecular weights. *Journal of Colloid and Interface Science* **336** (1), 360–367.

GORKOV, L. P. 1962 On the Forces Acting on a Small Particle in an Acoustical Field in an Ideal Fluid. *Soviet Physics Doklady* **6**, 773.

HAHN, PHILIPP, LEIBACHER, IVO, BAASCH, THIERRY & DUAL, JURG 2015 Numerical simulation of acoustofluidic manipulation by radiation forces and acoustic streaming for complex particles. *Lab on a Chip* **15** (22), 4302–4313.

HINTERMULLER, MARCUS A., REICHEL, ERWIN K. & JAKOBY, BERNHARD 2017 Modeling of acoustic streaming in viscoelastic fluids. In *2017 IEEE SENSORS*. IEEE.

KARLSEN, JONAS T. & BRUUS, HENRIK 2015 Forces acting on a small particle in an acoustical field in a thermoviscous fluid. *Physical Review E* **92** (4).

MULLER, PETER BARKHOLT & BRUUS, HENRIK 2014 Numerical study of thermoviscous effects in ultrasound-induced acoustic streaming in microchannels. *Physical Review E* **90** (4).

ROUSE, PRINCE E. 1953 A theory of the linear viscoelastic properties of dilute solutions of coiling polymers. *The Journal of Chemical Physics* **21** (7), 1272–1280.

SETTNES, MIKKEL & BRUUS, HENRIK 2012 Forces acting on a small particle in an acoustical field in a viscous fluid. *Physical Review E* **85** (1).

TIRTAATMADJA, V., McKINLEY, H. G. & COOPER-WHITE, J. J. 2006 Drop formation and breakup of low viscosity elastic fluids: Effects of molecular weight and concentration. *Physics of Fluids* **18** (4).

ZIMM, BRUNO H. 1956 Dynamics of polymer molecules in dilute solution: Viscoelasticity, flow birefringence and dielectric loss. *The Journal of Chemical Physics* **24** (2), 269–278.